Evolutionarily diverse LIM domain-containing proteins bind stressed actin filaments through a conserved mechanism

Jonathan D. Winkelman[a,1,2], Caitlin A. Anderson[b,1], Cristian Suarez[b], David R. Kovar[b,c,2], and Margaret L. Gardel[a,d,e,f,2]

[a]Institute for Biophysical Dynamics, University of Chicago, Chicago, IL 60637; [b]Department of Molecular Genetics and Cell Biology, University of Chicago, Chicago, IL 60637; [c]Department of Biochemistry and Molecular Biology, University of Chicago, Chicago, IL 60637; [d]James Franck Institute, University of Chicago, Chicago, IL 60637; [e]Physics Department, University of Chicago, Chicago, IL 60637; and [f]Pritzker School of Molecular Engineering, University of Chicago, Chicago, IL 60637

Edited by Laurent Blanchoin, Interdisciplinary Research Institute of Grenoble, Grenoble, France, and accepted by Editorial Board Member Yale E. Goldman August 27, 2020 (received for review March 11, 2020)

The actin cytoskeleton assembles into diverse load-bearing networks, including stress fibers (SFs), muscle sarcomeres, and the cytokinetic ring to both generate and sense mechanical forces. The LIM (Lin11, Isl- 1, and Mec-3) domain family is functionally diverse, but most members can associate with the actin cytoskeleton with apparent force sensitivity. Zyxin rapidly localizes via its LIM domains to failing SFs in cells, known as strain sites, to initiate SF repair and maintain mechanical homeostasis. The mechanism by which these LIM domains associate with stress fiber strain sites (SFSS) is not known. Additionally, it is unknown how widespread strain sensing is within the LIM protein family. We identify that the LIM domain-containing region of 18 proteins from the Zyxin, Paxillin, Tes, and Enigma proteins accumulate to SFSS. Moreover, the LIM domain region from the fission yeast protein paxillin like 1 (Pxl1) also localizes to SFSS in mammalian cells, suggesting that the strain sensing mechanism is ancient and highly conserved. We then used sequence and domain analysis to demonstrate that tandem LIM domains contribute additively, for SFSS localization. Employing in vitro reconstitution, we show that the LIM domain-containing region from mammalian zyxin and fission yeast Pxl1 binds to mechanically stressed F-actin networks but does not associate with relaxed actin filaments. We propose that tandem LIM domains recognize an F-actin conformation that is rare in the relaxed state but is enriched in the presence of mechanical stress.

cell mechanosensing | actin cytoskeleton | myosin

Cells are subject to a wide range of omnipresent mechanical stimuli, which play essential physiological roles. Epithelial tissue stretch modulates cell proliferation (1, 2), blood pressure regulates the contractility of endothelial cells within blood vessels (3, 4), and muscle contraction shapes connective tissue remodeling (5). Such mechanotransduction pathways allow for the integration of mechanical cues with the biochemical and genetic circuitry of the cell. While much progress has been made to elucidate the importance of mechanical stimuli in cell physiology, the underlying force-sensing mechanisms and organizational logic of many mechanotransduction pathways are unknown.

To respond to mechanical cues and dynamically modulate cell mechanics, the actin cytoskeleton exploits force-sensitive biochemistry to construct actin filament (F-actin)-based network assemblies. Focal adhesions, the adhesive organelles between cells and their external matrix, can change in composition and size under varied mechanical load (6). At the molecular scale, these focal adhesion changes arise primarily from force-dependent modulation of constituent proteins (6–8). The force-dependent association of the focal adhesion proteins, vinculin and talin, to actin filaments is sensitive to filament polarity (9, 10), providing a mechanism to guide local cytoskeletal architecture under load. Protrusive forces at the leading edge of migrating cells are generated by actin polymerization into short-branched F-actin networks (11). Compressive stress increases the actin filament density, which, in turn, alters its force generation potential (12). At the molecular scale, this mechanical adaptation of lamellipodial networks may arise from increased branch formation efficiency by the actin nucleator Arp2/3 complex on extensionally strained sides of bent actin filaments (13). Although cofilin was reported to have a reduced affinity for tensed actin filaments (14), this has recently been called into question (15). While direct evidence for detection of stressed actin by actin-binding proteins is still scant, the structural polymorphism in actin filaments suggests that force-induced conformations exist and could be recognized by actin-binding proteins (16). There may be information about the mechanical state of the cell stored within these actin filament conformations available to be read by actin-binding proteins that regulate various mechanotransduction pathways.

Within adherent cells, F-actin bundles known as stress fibers (SFs) generate contractile force across the cell and, via focal adhesions, are coupled to the extracellular matrix. SFs dynamically rearrange over long (hour) time scales in response to forces applied to the extracellular matrix (17), and this remodeling

Significance

Genes encoding LIM domains underwent a large expansion in animals. These LIM domain-containing proteins are functionally diverse and involved in a variety of fundamental cellular processes. Previous work suggests that many are sensitive to mechanical forces experienced by the cell. This study finds that many of these proteins in animals detect stressed cytoskeletal networks in cells by directly binding to a stretched conformation of the actin filament. This mechanism of force sensing by LIM within the cell is conserved from yeasts to mammals. This work suggests the possibility that a variety of biological pathways may be regulated by LIM domain detection of strained actin filaments.

Author contributions: J.D.W., C.A.A., C.S., D.R.K., and M.L.G. designed research; J.D.W., C.A.A., and C.S. performed research; J.D.W., C.A.A., C.S., D.R.K., and M.L.G. contributed new reagents/analytic tools; J.D.W., C.A.A., and C.S. analyzed data; and J.D.W., C.A.A., D.R.K., and M.L.G. wrote the paper.

The authors declare no competing interest.

This article is a PNAS Direct Submission. L.B. is a guest editor invited by the Editorial Board.

[1]J.D.W. and C.A.A. contributed equally to this work.

[2]To whom correspondence may be addressed. Email: jon.winkelman@gmail.com, drkovar@uchicago.edu, or gardel@uchicago.edu.

This article contains supporting information online at https://www.pnas.org/lookup/suppl/doi:10.1073/pnas.2004656117/-/DCSupplemental.

First published September 28, 2020.

process requires zyxin and paxillin (17–21). At short times, mechanical failure of the SF can occur either spontaneously or in response to applied force (18, 20). At such damage sites, the SF is locally weaker, leading to a localized retraction to create a stress fiber strain site (SFSS) (20) (Fig. 1*A*). Rather than irreversible failure, a repair process at the SFSS is initiated by the rapid accumulation of zyxin and followed by the recruitment of binding partners VASP and α-actinin to promote actin assembly and cross-linking to repair the SF and maintain mechanical homeostasis (20) (Fig. 1*A*). The recruitment of VASP and α-actinin require known interactions at the zyxin N terminus (21). However, the recruitment of zyxin to the SFSS occurs through a region near the C terminus that contains three tandem Lin11, Isl-1, and Mec-3 (LIM) domains separated by two short 7- to 8-residue-length unstructured linkers (Fig. 1 *B* and *C*) (20). While this LIM domain-containing region (LCR) is necessary and sufficient for localization to the SFSS, the underlying mechanism is not known. It has been speculated that the signal within the SFSS that the LCR senses may arise from new F-actin barbed ends, conformational changes to an actin-binding protein, or posttranslational modifications of actin or zyxin's binding partners (21). Moreover, the focal adhesion protein paxillin also localizes to the SFSS through its LCR (18), suggesting that this apparent mechanosensing process may be more generally conserved.

The family of proteins that contain one or more LIM domains is large. In humans, there are ∼70 genes containing LIM domains that can be divided into 14 classes (22), many of which associate with load-bearing elements of the cytoskeleton, such as focal adhesions, cell–cell adhesions, and stress fibers (21). There are at least 26 LIM domain-containing proteins that localize to focal adhesions, many of which require cell contractility for proper localization (7, 8). While LIM domain-containing proteins are ubiquitous in diverse mechanotransduction pathways, it is unknown whether these share a mechanism by which mechanical stimuli is transduced. Moreover, the mechanism by which the LCR is recruited to the SFSS is unknown.

We employed a combination of live cell imaging and in vitro reconstitution approaches to explore cytoskeletal mechanosensing by LIM domain proteins. We first established a SFSS-localization screen of diverse LCRs from both mammals and yeast and identified 18 LCRs within the Zyxin, Paxillin, Tes, and Enigma LIM protein classes that bound to the SFSS. We also determined that paxillin-like 1 (Pxl1) from fission yeast localizes to the SFSS in mammalian cells, suggesting that the strain-activated target produced in the SFSS and recognized by LCRs is well conserved. Sequence and domain analysis of SFSS-binding LCRs shows that tandem LIM domains contribute additively to SFSS association. To identify the strain-activated target of LCR, we reconstituted contractile actomyosin networks in vitro and observed LCR localization to mechanically stressed actin filaments. From these data, we propose that tandem LIM domains bind a periodic molecular mark that emerges on strained actin filaments.

Results

LCRs from Diverse Mammalian Proteins Bind to SFSS. SFs are contractile bundles of 10 to 30 cross-linked actin filaments with alternating bands enriched with either myosin II motor or α-actinin, VASP, and zyxin (Fig. 1*A*) (21), a structure similar to that in striated myofibrils (23). SFSS develop when SFs mechanically fail, resulting in local elongation and thinning that compromise their force transmission (20) (Fig. 1 *A* and *D–F*). Zyxin rapidly accumulates at the SFSS and recruits the actin assembly factor VASP and cross-linking protein α-actinin to repair and stabilize the damaged site (Fig. 1*A*) (20). Previous work identified the LCR of zyxin to be necessary and sufficient for accumulation on the SFSS (18). Measuring the fluorescence intensity of zyxin and actin along the SF prior to a SFSS reveals locally diminished intensity of both proteins at the future SFSS (Fig. 1 *D–F*). Examining the local actin intensity of a future SFSS, we find that the actin intensity is depleted fivefold as compared to regions of SFs that do not fail (Fig. 1 *F* and *G* and Movie S1). Moreover, we find that >65% of SFSSs occur in a myosin-rich band (Fig. 1*H*), and myosin II is displaced laterally from the SFSS (*SI Appendix*, Fig. S1 *A–C*). The filament density decreases as the SFSS expands (20), and zyxin recruitment occurs nearly simultaneously as the length L of the strain site increases (Fig. 1*I*). For temporal alignment of data, we define t = 0 as the time of zyxin accumulation (Fig. 1 *F* and *I*). These data suggest that SFSSs occur at SF regions predisposed to failure because of lower actin density and depletion of actin assembly and cross-linking factors. We also found that SFSSs can be induced by partially damaging the SF with high laser intensity (Fig. 1*J* and Movie S2). The LCR of zyxin is recruited to laser-induced SFSSs with similar kinetics to that of spontaneous SFSSs (Fig. 1*K* and *SI Appendix*, Fig. S1*D*). Considering force balance along the SF in either of these two scenarios, the reduced number of actin filaments at the SFSS suggests filaments and cross-links present there are under an increased load.

To assess whether localization to the SFSS is a feature ubiquitous within the LIM family of proteins, we developed an assay to quantify their recruitment to either endogenous or induced SFSSs. We cloned the LCR from one or more genes belonging to each LIM protein class (22) and generated mCherry-tagged mammalian expression constructs. Each of the 28 mCherry-tagged LCRs was transiently transfected into mouse embryo fibroblast (MEF) cells with GFP-zyxin stably integrated into the genome. Using the GFP-zyxin as a positive marker for SFSSs, we then assessed the localization of the mCherry-tagged LCRs at the site (Fig. 1*K*). As a control, the mCherry-tagged constructs of both full-length zyxin and the LCR of zyxin, LCR(zyx), localize very similarly to GFP-zyxin (Fig. 1 *K* and *L* and Movie S3). At a SFSS, we generated kymographs (Fig. 1*K*) and, from these, took linescans across the time axis at the center of the SFSS to generate a kinetic profile of SFSS accumulation for both GFP-zyxin and the transfected LCR-mCherry. From these profiles, the ratio of the LCR-mCherry to GFP-zyxin was determined and normalized (*SI Appendix*, Fig. S1 *E–N*) such that a cytoplasmically expressed mCherry-tagged nuclear export signal (NES), which was added to all LCRs, is zero and mCherry-LCR(zyx) is one (Fig. 1*L*). Ratio averages that were significantly above zero were scored as SFSS binders. We observed SFSS localization of the LCRs from 18 proteins across four LIM classes: Zyxin, Paxillin, Tes, and Enigma (Fig. 1 *L* and *M*). SFSS sensing is isolated to, but ubiquitous within, these classes. The LCRs of all but two protein subgroups tested from these classes (Lmcd1 and Alp) localize to SFSSs significantly above background. These results identify novel LIM domain protein sensitivity to mechanical strain in the actin cytoskeleton and demonstrate its conserved function across diverse LIM domain-containing proteins.

LIM Domains from Fission Yeast Bind to SFSS in Mammalian Cells Via a Conserved Mechanism. To explore when SFSS binding arose in LIM domain proteins along evolutionary lines and to determine the level of conservation, we looked for SFSS-binding homologs in more divergent species. The Paxillin class first appears in the unikonts (amoebas, yeasts, and metazoans) while Tes, Zyxin, and Enigma classes arose later in the metazoans (22). Reflecting a much simpler genome, the fission yeast *Schizosaccharomyces pombe* expresses five LIM domain-containing proteins: Rga1, Rga3, Rga4, Hel2, and Pxl1 (Fig. 2*A*). The only contractile actin filament network in fission yeast is the cytokinetic ring, where

myosin-rich nodes condense into an actomyosin bundle that constricts to drive cell division (24). Time-lapse imaging of fission yeast Pxl1-GFP shows strong colocalization with myosin II at the contractile ring but only after the ring has assembled and begins to constrict (Fig. 2*B*) (25, 26). Although localization to the constricting contractile ring may suggest mechanosensitive localization, we could not easily manipulate the mechanics of the ring to directly test this possibility.

To determine whether SFSS localization found in mammalian LCRs is preserved in the fission yeast LIM domain-containing proteins, we used the SFSS-localization assay developed for mammalian cells. We transfected fission yeast LCRs tagged with mCherry into MEF cells containing stably integrated GFP-zyxin. The LCR of fission yeast Pxl1, LCR(Pxl1), localizes with the periodic z-bands in SFs but is largely absent from focal adhesions (Fig. 2*C*). Surprisingly, LCR(Pxl1) exhibits strong SFSS localization, similar to that observed with LCR(zyx) (Fig. 2 *C–E* and Movie S4). Conversely, the LCR of fission yeast RhoGAPs and budding yeast Pxl1 did not display SFSS localization (Fig. 2*E*). To determine if the fission yeast LCR(Pxl1) binds to the same target in SFSS as mammalian LCR(zyx), we compared their accumulation kinetics at the SFSS (Fig. 2*F*) and calculated the time to reach half of the maximum fluorescence intensity ($t_{1/2}$). The $t_{1/2}$ of LCR(Pxl1) is nearly identical to LCR(zyx) (Fig. 2*F*), strongly suggesting that the two highly divergent LCRs use the same mechanism for SFSS association.

As a second test of whether LCR(Pxl1) and LCR(zyx) sense the same binding site to associate with the SFSS, we assayed whether they compete for association to the same SFSS. For these experiments, we exploited natural variations in the expression of zyxin-GFP and LCR(Pxl1)-mCherry in our cell populations (Fig. 2 *G–I*). As expected, cells expressing high levels of zyxin showed more zyxin signal at the SFSS (Fig. 2*H*), which is also true for LCR(Pxl1) (*SI Appendix*, Fig. S2*A*). We also verified that expression of zyxin is not correlated with expression of LCR(Pxl1) (Fig. 2 *I*, *Inset*). Importantly, high zyxin expression inversely correlates with reduced SFSS association of LCR(Pxl1) (Fig. 2 *H* and *J*). For instance, when expressed at low levels, zyxin accumulation at SFSS is nearly completely inhibited by LCR(Pxl1) (Fig. 2 *G* and *I*), and conversely, very little LCR(Pxl1) accumulates at the SFSS in cells expressing high levels of zyxin (Fig. 2*I*). The competitive relationship between zyxin and LCR(Pxl1) argues that these diverse LCRs (*SI Appendix*, Fig. S2 *B* and *C*) are recruited to the SFSS via the same mechanism. Although yeasts may not have canonical SFs, the contractile ring may still exhibit processes similar to SFSS (26, 27) that are recognized by Pxl1. Thus, although fission yeast do not contain SFs, a highly conserved molecular feature that exists in both fission yeast and mammalian SFSS is recognized by LCR(Pxl1). We conclude that the target of SFSS-sensing LCRs existed in the common ancestor of yeast and mammalian cells, and this association of LCRs with the actin cytoskeleton has likely been conserved since at least the divergence of yeasts and mammals.

Tandem LIM Domains Contribute Additively to SFSS Localization. Since LCRs from mammals and fission yeast appear to recognize a common target in SFSS, we speculated that conserved amino acid (AA) sequence signatures may be required for this function. Within the LCR of zyxin, there are three LIM domains (LIM1, LIM2, and LIM3) separated by two short linkers (Fig. 1*C*). Outside of the highly conserved amino acids that coordinate the zinc ions (Cys, His, or Asp), the sequences of individual LIM domains are highly variable. For instance, LIM2 and LIM3 share only 33% and 26% sequence identity to LIM1 (Fig. 3*A*). Furthermore, LCRs from SFSS-binding and -nonbinding proteins show a similar level of sequence identity (30% and 28%) to LIM1 of zyxin (Fig. 3*A*). Despite this sequence diversity, results complementary to ours show that a phenylalanine at position 66 (F66) of the LIM domains in Zyxin, Hic5, and FHL3 is necessary for localization to tensed actin filament networks both in cells and in vitro (28). Among LIM domains from SFSS sensors, only 75% of these contain F66 (*SI Appendix*, Fig. S3 *A–C*); it is possible that proximal phenylalanine or tyrosine residues may be a suitable substitute (*SI Appendix*, Fig. S3*B*). However, 29% of the nonbinders also have an F66, indicating that this amino acid is not sufficient for SFSS binding (*SI Appendix*, Fig. S3 *B* and *D*). This led us to focus on other features of the LCR involved in SFSS localization. We noticed common organizational elements of the LCR in SFSS binders. First, all SFSS binders contain three or more LIM domains in tandem organization, while 85% of nonbinders have fewer than three LIM domains (Fig. 3*B*). For all mammalian and yeast proteins in Zyxin, Paxillin, Tes, and Enigma classes, we plotted the level SFSS binding determined from the screens in Figs. 1*M* and 2*E* versus the number of LIM domains within the LCR. We found that the degree of SFSS binding is weakly correlated ($R^2 = 0.7$) with the number of tandem LIM domains (Fig. 3*C*). Furthermore, linkers from SFSS-binding proteins are 7 to 8 amino acids long, while linkers in nonbinders range widely from 7 to 200 amino acids (Fig. 3*D*). These findings suggest a testable hypothesis that tandem LIM domains connected by a short linker is necessary for SFSS binding (Fig. 3*E*).

We addressed these possibilities by exploring how alterations to LCR(zyx) organization impacts its localization to SFSS using the screening approach described previously. Constructs containing any one LIM domain of zyxin, denoted as LIM1(×1), LIM2(×1), or LIM3(×1), do not localize to the SFSS (Fig. 3*F*). However, linkage of multiple LIM1 domains in tandem connected by a linker 8 AA long (*Materials and Methods*) are recruited to the SFSS (Fig. 3*F*). Two tandemly linked LIM domains, denoted as LIM1(×2), LIM3(×2), and LIM1LIM2, weakly associate with SFSS (Fig. 3*F* and *SI Appendix*, Fig. S4 *A* and *B*). Additionally, three tandemly linked LIM domains, denoted by LIM1(×3) or LIM3(×3), exhibit SFSS localization similarly as well as LCR(zyx) (Fig. 3*F*). When the number of LIM1 repeats is increased to four, LIM1(×4), or five, LIM1(×5), the localization to the SFSS further increases, exceeding LCR(zyx) by up to twofold (Fig. 3*F*). These data suggest that each LIM domain alone may weakly bind the target within the SFSS, but multiple interactions (at least for LIM1 and LIM3) contribute to the avidity of target binding. To determine whether the specific organization of LIM oligomerization matters, we clustered four LIM1 in parallel with a synthetic GCN4 tetramerization domain (TD) that drives the formation of a left-handed coiled coil (29), TD-LIM1(×4). However, we did not observe SFSS localization with this construct (Fig. 3*F*). Since the length of linkers in SFSS-binding LCRs is highly conserved (Fig. 3*D*), we tripled the linker lengths in LCR(zyx) from 8 to 24 amino acids (long linker), which abrogated SFSS localization (Fig. 3*F*). Thus, full binding of LCR to the target within the SFSS requires at least three tandem LIM domains connected with a short linker. We note that the Pinch and Ablim classes both contain more than three tandem LIM domains but fail to localize to the SFSS in our screen. This could be explained by the fact that in both classes 1) two of the LIMs are connected by a longer (13 to 19 AAs) linker, and 2) the central LIM domain does not contain an F or similar amino acid at position 66 to 70. This supports the notion that a serial organization of multiple, appropriately spaced LIM domains is necessary for SFSS binding.

In Vitro Reconstitution of LCR Recruitment to Contractile Actomyosin Bundles. While the above experiments identify organizational features of the LCR required for association with the SFSS, its

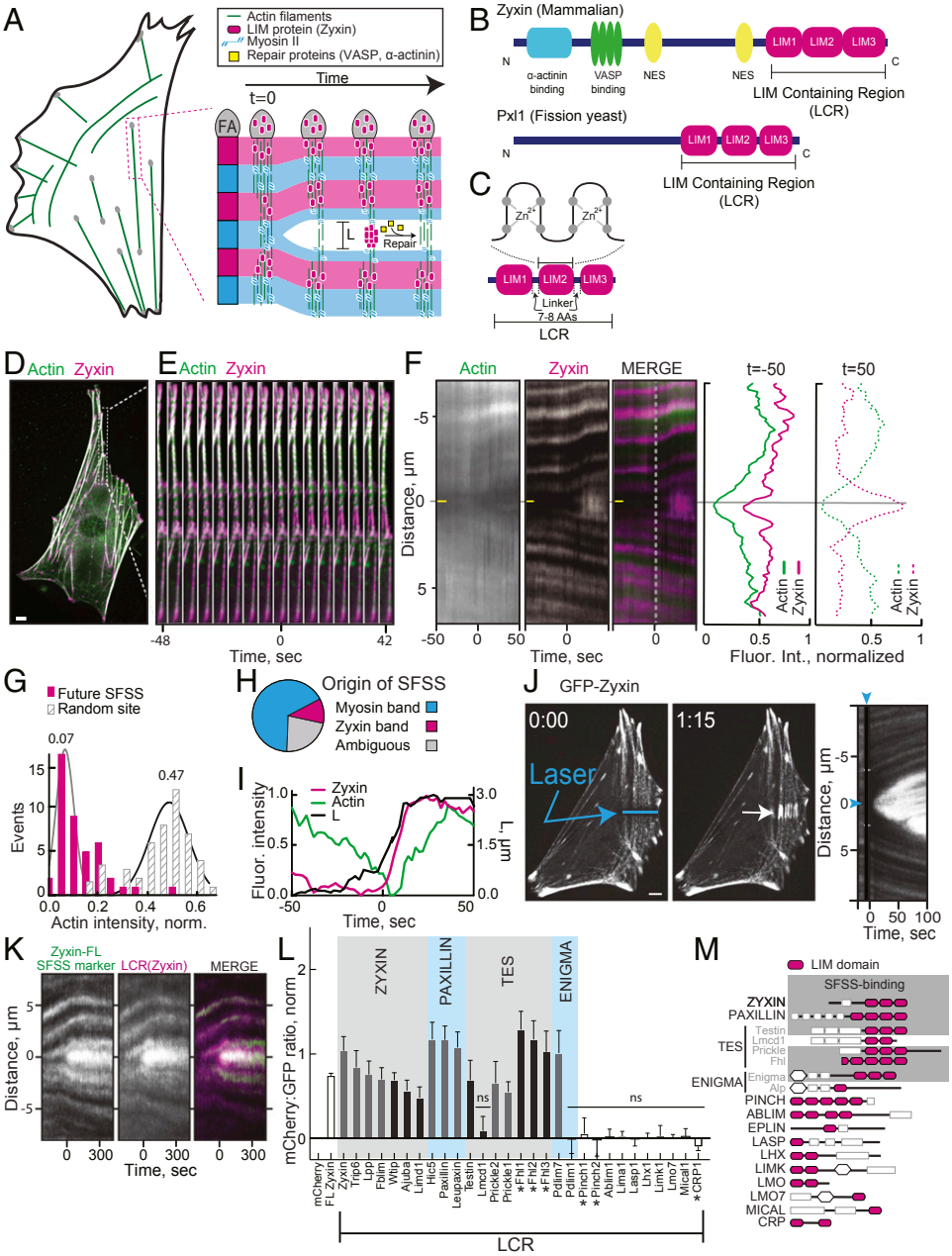

Fig. 1. Diverse LIM domains localize to SFSS. (*A*) Cartoon of a fibroblast cell with actin stress fibers. Schematic of the development and repair of a SFSS. FA, focal adhesion; L, distance (length) across the SFSS. (*B*) Domain organization of the LIM domain (pink ovals)-containing proteins mammalian zyxin and fission yeast Pxl1. Zyxin also contains binding sites for α-actinin (F-actin cross-linker) and VASP (F-actin elongation factor), and two nuclear export sequences (NESs). LCRs are indicated. (*C*) Each LIM domain contains two zinc finger binding domains with conserved residues (cysteine/histidine, gray circles) to chelate the zinc, but the remaining sequence varies between different LIM domains. The linker length between adjacent LIM domains is 7 to 8 amino acids. (*D–I*) Analysis of SFSS in MEFs with stably integrated GFP-zyxin and transfected mApple-actin. (Scale bar, 5 µm.) (*D* and *E*) Fluorescent micrograph (*D*) and associated montage (*E*) of a representative stress fiber over time showing accumulation of zyxin on a developing SFSS. (*F*, *Left*) Kymographs of the same event: actin channel (*Left*), zyxin channel (*Middle*), and a merged image (*Right*). The future SSFS (horizontal yellow line) indicates where background measurements for (*G*) and a later screen will be taken. Vertical dotted line indicates when strain has begun at t = 0. (*F*, *Right*) Average fluorescence intensity line scans of 74 SFSS, measured 50 s before and after initiation. (*G*) Histogram of actin intensities at a future SFSS (~50 s prior) and random sites on the same stress fiber. (*H*) Pie chart showing the distribution of where SFSS occurred. (*I*) Kinetics of zyxin accumulation and actin depletion and reassembly (*Left y* axis), and distance across the SFSS indicated as L in *A* (*Right y* axis), for a representative SFSS. (*J*, *Left*) Fluorescent micrographs showing laser induction of a SFSS in a representative MEF cell with stably integrated GFP-zyxin. Blue line shows where light was targeted, and white arrow denotes developing SFSS. (Scale bar, 5 µm.) (*J*, *Right*) Kymograph showing this event over time, with blue arrowheads indicating time and location of laser light. (*K*) Representative kymograph of the laser-induced SFSS screen, from a cell expressing GFP-zyxin and LCR(zyxin)-mCherry. (*L*) Screen of 29 LIM domain proteins from *Mus musculus*. The *y* axis is the mCherry:GFP ratio at the strain site, error bars = 95% CI, $n > 6$ per LCR construct except Prickle1-2 and Limd1 where $n > 2$ cells respectively. n = average taken from a single cell, usually with multiple SFSS measurements taken in each cell. Proteins not significantly different from background (mCherry alone) in ANOVA test are denoted as not significant (ns). LCR constructs were used for all but those marked with *, for which the whole protein sequence was used. Labels above graph denote the broader LIM class from which each protein belongs. (*M*) Domain organizations of LIM classes of proteins in mammals. Gray box denotes SFSS-binding families. Two classes, TES and ENIGMA, contained subgroups that did not bind SFSS, Lmcd1, and Alp.

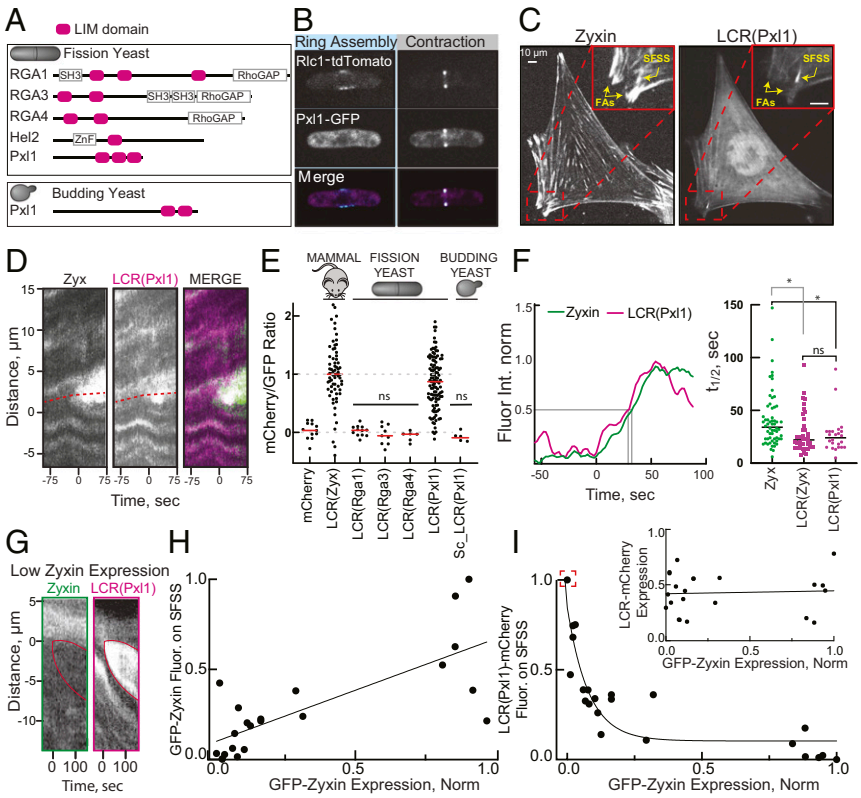

Fig. 2. LCR of fission yeast Pxl1 associates to the SFSS and displays similar kinetics and competes at the SFSS. (*A*) Domain organization of *S. pombe* (fission yeast) LIM domain proteins and budding yeast Paxillin-like 1 (Pxl1). (*B*) Fluorescent micrographs of a fission yeast cell undergoing cytokinesis that is expressing myosin II regulatory light chain Rlc1-tdTomato and full-length Pxl1-GFP. Contractile ring assembly (*Left*) and beginning of contraction (*Right*) are shown. (*C*) MEF cell expressing GFP-zyxin and the LIM domains of fission yeast Pxl1, LCR(Pxl1)-mCherry. Focal adhesions (FAs) and SFSS (yellow arrows) are labeled in the magnified *Inset* image. (*D*) Kymograph of SFSS in the MEF cell from *C*. (*E*) Screen for SFSS association in fission yeast and budding yeast LCRs. Each LCR mCherry:GFP ratio was compared to background with ANOVA, ns, not significantly different. Each point represents individual SFSS ratio, *n* = average cellular ratio of 1 or more SFSS, 4 < n < 30. (*F*, *Left*) Plot of the accumulation of GFP-zyxin and fission yeast LCR(Pxl1)-mCherry on SFSS over time. Gray lines indicate $t_{1/2}$ for GFP and mCherry. (*F*, *Right*) Plot of $t_{1/2}$ for accumulation on SFSS. Asterisks indicate statistical significance; ns, not significant as determined by ANOVA, *n* = 60, 24, 38. (*G–I*) Fluorescence intensity of zyxin and LCR(Pxl1) at SFSS correlates with expression levels. (*G*) Kymograph showing competition of fission yeast LCR(Pxl1)-mCherry with GFP-zyxin at a MEF cell SFSS. Expression levels were estimated by measuring cytoplasmic intensity. (*H*) Fluorescence signal of fission yeast LCR(Pxl1)-mCherry or GFP-zyxin at SFSS as a function of estimated expression levels of the same construct. $R^2 = 0.57$, $n = 21$. (*I*) Fluorescence signal of LCR(Pxl1) at SFSS as a function of estimated expression of GFP-zyxin. $R^2 = 0.81$. (*I*, *Inset*) Estimated expression of LCR(Pxl1)-mCherry as a function of GFP-zyxin expression. $R^2 = 0.003$.

binding target remains unclear. These experiments also indicate that LCR binding to the SFSS is highly conserved from mammals to fission yeast, suggesting the binding target of the LCR may be a core component of the eukaryotic contractile machinery. To identify the target within SFSS that is recognized by LCRs, we chose an in vitro reconstitution approach with a well-studied set of purified proteins. Untagged and SNAP-tagged LCR proteins SNAP-LCR(Pxl1) and SNAP-LCR(zyx) (Fig. 4*A* and *SI Appendix*, Fig. S5*A*) were purified from bacteria and the SNAP tag was fluorescently labeled with SNAP-surface 549 or 647 for single molecule imaging using total internal reflection fluorescence (TIRF) microscopy. Untagged and SNAP-tagged LCR(zyx) and LCR(Pxl1) elute from a gel filtration column as a stable monomer.

A leading hypothesis is that LCR(zyx) binds to actin filament barbed ends produced from filament breakage in the SFSS (20). We first tested whether LCR(zyx) or LCR(Pxl1) binds to actin filament sides or barbed ends in standard bulk assays (*SI Appendix*, Fig. S5 *B* and *C*). Actin filament sedimentation assays revealed a barely detectable increase of either the LCR in the pellet over a range of increasing actin filament concentrations, indicating an extremely weak affinity for actin filaments (*SI Appendix*, Fig. S5*B*). To query for F-actin barbed end binding, we utilized a seeded pyrene actin assembly assay to measure relative rates of elongation. Protein binding to assembling barbed ends usually modulates their elongation rates (11, 30), but we failed to detect any change in the presence of LCRs (*SI Appendix*, Fig. S5*C*). In support of these bulk biochemical assays, imaging of fluorescently labeled SNAP-LCR shows very minimal colocalization with actin filaments via TIRF microscopy (TIRFM) (Fig. 4*F*; −27 and −23 min). Thus, the LCR appears to have a very low affinity to the sides or the barbed ends of relaxed actin filaments.

Since Pxl1 and zyxin localize to diverse actomyosin contractile structures, we hypothesized that these LCRs bind to an element common to both fission yeast contractile rings and mammalian SFs. We reconstituted the core contractile machinery base on previously developed protocols (31, 32). An F-actin network was assembled from actin monomers, α-actinin, and a SNAP-LCR [LCR(Zyx) or LCR(Pxl1)], within a buffer that contained 0.5% methylcellulose to crowd the network to a polyethylene glycol (PEG)-passivated glass coverslip surface. Individual actin filaments are mobile, but dynamics arrest as filaments elongate and are cross-linked by α-actinin into a network of mixed polarity bundles (Fig. 4*B*; 0 min). When the network reached an appropriate density, we flowed in a fresh mixture containing the initial concentrations of SNAP-LCR and α-actinin, the critical concentration

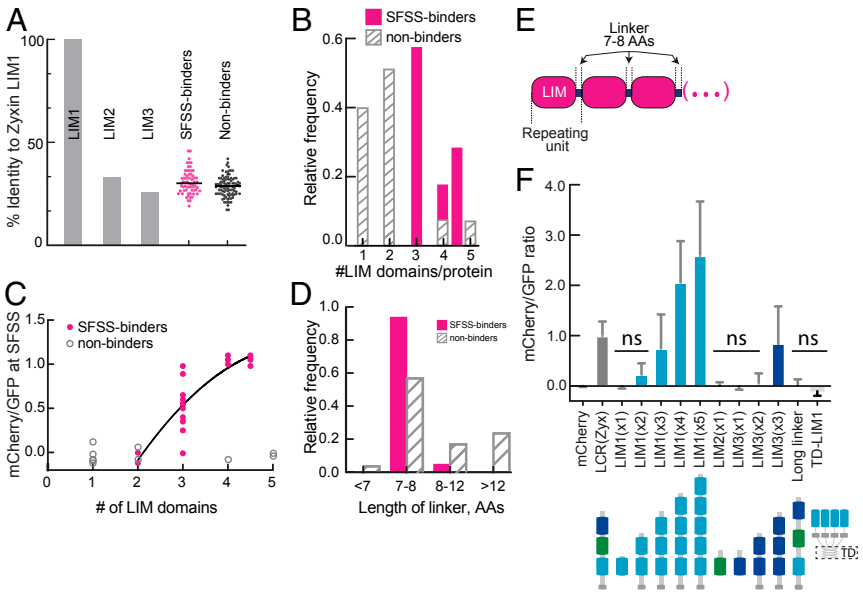

Fig. 3. LCRs bind to SFSS through multiple, precisely spaced domains organized in tandem. (*A*) Amino acid identity to mammalian zyxin's first LIM domain (LIM1) of zyxin's other LIM domains (LIM2 and LIM3) and LIM domains from SFSS-binder and -nonbinder classes. (*B*) Histogram of the number of individual LIM domains in each SFSS-binder and -nonbinder protein. (*C–E*) Common organizational elements of LCRs in SFSS binders. (*C*) Plot of SFSS binding vs. the number of LIM domains in the LCR construct. Data from LCRs within LIM-binding classes was fit with a quadratic function using least squares. $R^2 = 0.68$. (*D*) Length distribution of linkers (in amino acids) connecting LIM domains in SFSS-binding (55 linkers) and -nonbinding classes (47 linkers) (*E*) Domain organization of a typical SFSS-binding LCR. There are typically three (or more) LIM domains separated by linkers of 7 to 8 residues. (*F*) SFSS-association screen of various organizations of zyxin's LCR. LIM1(×3) indicates the LIM1 is repeated three times. TD-LIM1 indicates the LIM1 domain was oligomerized by the addition of a modified GCN4 tetramerization domain (TD); ns, not significantly different from background as determined by ANOVA. $5 < n < 15$; n = average cellular ratio of one or more SFSS.

of actin monomers (0.1 μM) to prevent network disassembly, and prepolymerized myosin II filaments (Fig. 4*B*; 30 min). Myosin II activity on F-actin generates local stresses and deformations that remodel and contract the network. Gently curved bundles become taut, with many breaking over time (Fig. 4*B*; 31 min and Movie S5). These failures usually occurred at bundle junctions ("T-junctions") and more rarely along the length of a single filament or bundle (~10%). After rupture, bundle portions recoil and then compact into asters in which actin filaments are compressed, bent, and severed (31). Thus, the myosin-driven contraction of a reconstituted F-actin network occurs with a buildup of both tensile and compressive stresses on the actin filaments that drive filament buckling and breaking (31).

Whereas the LCR does not localize well to the networks initially, consistent with the "bulk" F-actin sedimentation assays (*SI Appendix*, Fig. S5*B*), after the addition of myosin II, the LCR accumulates on a subset of the network structures most likely to be under high contractile tension (Fig. 4 *C–L* and Movies S6 and S7). The majority (~90%) of myosin II-induced breaks in the network occurred at T-junctions (Fig. 4 *C* and *D*) where actin filaments become highly distorted and break. Assuming the number of filaments in a bundle is constant and forces are balanced, there should not be increased tension at the T-junction compared to more distal sites along the filament bundle. However, filaments at these junctions are highly curved, which could also be coupled to changes in filament twist (33). Further work is needed to understand the underlying mechanism of LCR recruitment.

LCRs bind more frequently to T-junctions that break than to nonbreaking T-junctions and random sites along the actin network (Fig. 4 *C* and *D* and Movie S5). A majority of the T-junction breaks appear to bind single molecules of LCR (Fig. 4 *C*, *Left*), but there is a fraction of T-junctions that show increasing LCR fluorescence prior to breaking (Fig. 4 *C*, *Right*). To verify that we are observing single molecules, we monitored LCR bleaching in our experiments and obtained the average fluorescence intensity of a single dye. A total of 78% of the LCR puncta monitored disappeared in a single step (*SI Appendix*, Fig. S5*D*). A distribution of the maximum LCR fluorescence intensity suggests that most T-junction bindings show fluorescence values consistent with that of single molecules of the LCR (Fig. 4*E*). To get a sense of the affinity of LIM domains for sites of stressed F-actin, we measured the residence time of LCR single molecule fluorescence on the two T-junction populations (breaking and nonbreaking). We monitored the residence time of LCR puncta on T-junctions that displayed fluorescence intensities consistent with single LCR molecules (*SI Appendix*, Fig. S5 *D*, *Right*). LCRs associate for an average of 30 s but the LCR signal disappears from the network coincident (at our 10-s imaging interval) with breaking of a T-junction (Fig. 4*F*). Since the average bleaching time is over 10-fold higher than the measured residence time, we conclude that the disappearance of signal at the T-junction is due to LCR dissociation rather than bleaching (*SI Appendix*, Fig. S5*E*). An assumption that the LCR association rate is between 10^6 and 10^7 M^{-1} s^{-1} (34) and the measured off rate of ~0.038 s^{-1} (1/residence time) (Fig. 4*F*) suggests that the LCR may have low nanomolar affinity for actin filament conformations that are enriched at T-junctions.

Compared to T-junctions, myosin-induced breaks along the F-actin bundle are much rarer. However, when these breaks occur, SNAP-LCR(Pxl1) binding to the bundles appears dynamic with most localization occurring within 5 min prior to breaking at t = 0 min (Fig. 4 *G* and *H*). While the exact localization site varies between breaking events, SNAP-LCR signal is detected for an average of 60% of the 5 min prior to bundle break (Fig. 4*I*). The LCR is also observed along control bundles that do

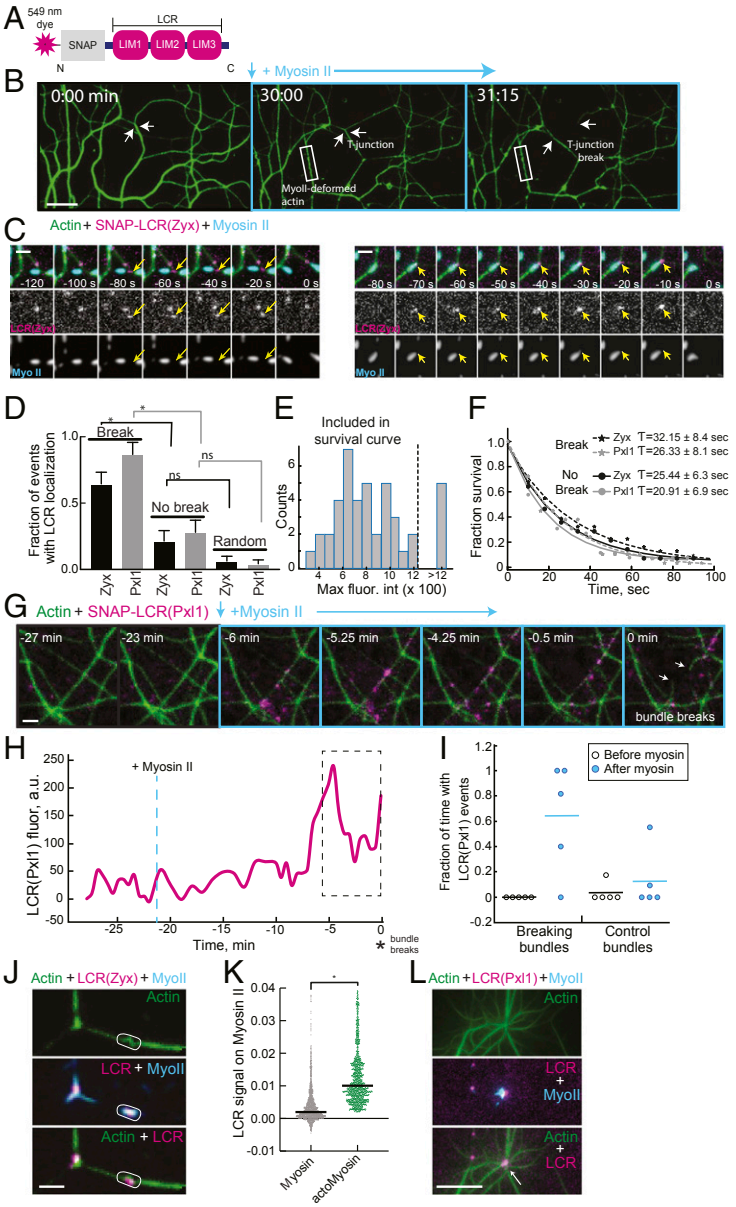

Fig. 4. Purified LCR of yeast Pxl1 and mammalian zyxin localized to stressed F-actin networks. (*A*) Schematic of the SNAP-tagged LCR protein constructs used for in vitro experiments. (*B–K*) TIRFM visualization of the recruitment of LCR protein constructs to actin filament networks. F-actin networks were preassembled with Mg-ATP-actin (10% Alexa-488 labeled), α-actinin, and the indicated LCR construct (SNAP-549 tagged) for 30 to 45 min. Network contraction was subsequently induced by flowing in polymerized myosin II with actin (0.1 μM) and the same initial concentrations of α-actinin and LCR. (*B*) Representative time lapse of the in vitro contraction assay. After myosin is added to the preassembled bundled F-actin network, several types of network stresses occur, including T-junctions (white arrow) and myosin-induced F-actin deformations (white box). (Scale bar, 10 μm.) (*C–F*) LCR localization to T-junctions. (*C*) Representative time-lapse montage. A preassembled network was formed with 1.5 μM actin, 75 nM α-actinin, and 100 nM SNAP-LCR(zyx), followed by the addition of 100 nM myosin to induce network contraction. Yellow arrows show when LCR(zyx) localizes to the T-junction prior to break. (Scale bar, 2 μm.) (*D*) Quantification of fraction of events where LCR signal was observed: at T-junctions in the frame before breaking (break), at T-junctions that did not break (no break), or at random sites along bundles (random). Error bars represent SEM, $n > 14$ events for each condition. ns = $P > 0.05$; *$P < 0.05$ as determined by ANOVA. (*E*) Distribution of maximum fluorescence intensity of LCR on a T-junction. Data to the *Right* of the dotted line were excluded from residence time calculations as shown in *F*. (*F*) Lifetime of LCR single molecules on T-junctions that broke (stars) or did not break (circles) average lifetimes derived from single exponential fits (lines). error = 95% CI calculated from curve fits, n = individual LCR-binding event, $n > 14$. (*G–I*) LCR localization to less common breaks along filament bundles. (*G*) Representative time-lapse montage of a preassembled network formed with 3.0 μM actin, 150 nM α-actinin, and 200 nM SNAP-LCR(Pxl1), followed by the addition of 75 nM skeletal muscle myosin II to induce network contraction. (Scale bar, 2 μm.) White arrows indicate broken ends of a bundle. (*H*) LCR(Pxl1) recruitment measured along the F-actin bundle in *G* that breaks at time 0. (*I*) LCR(Pxl1) fluorescence along bundles was measured similarly as in *H* for five bundle breaking events. Since LCR recruitment appears to be dynamic along the bundle, the fraction of frames with LCR localization during the 5 min just prior to the break was measured. (*J–L*) LCR localization to myosin along stressed F-actin networks, particularly where myosin deforms F-actin bundles. (*J*) Representative fluorescent image of LCR(zyx) localizing with myosin II along the network. Ovals indicate myosin on the F-actin network or on the glass. (Scale bar, 2 μm.) (*K*) Quantification of LCR localization with myosin or myosin associated with actin (actomyosin). n = individual myosin puncta in four different movies, $n > 300$, bar indicates mean; *$P < 0.05$ as determined from t test. (*L*) Representative fluorescent images of a large aster that forms from a preassembled network with 3.0 μM actin and 200 nM SNAP-LCR(Pxl1) in the absence of α-actinin, followed by the addition of 90 nM myosin II (Alexa-647 labeled). (Scale bar, 10 μm.) LCR(Pxl1) localizes to the center of these asters with the myosin (white arrow).

not break throughout the course of the movie, but for only an average of 20% of the 5 min (Fig. 4*I*). LCR(Pxl1) only associates to the network after myosin addition, remaining on filament portions for several minutes prior to breaking at t = 0 min (Fig. 4 *H* and *I*).

The LCR also colocalizes with myosin II, especially in areas with highly deformed F-actin networks (Fig. 4 *J*–*L* and Movie S7). While SNAP-LCR is detected above background on isolated myosin II (*SI Appendix*, Fig. S5*F*), LCR binding is approximately fivefold higher when myosin is localized on the F-actin network, suggesting this colocalization is a result of LCR binding to myosin-induced actin filament deformations rather than directly to myosin (Fig. 4*K*). Line scans of a bundle over time show that the majority of LCR localization is independent of myosin localization (*SI Appendix*, Fig. S6). This further indicates that colocalization of the LCR and myosin II along the network is due to LCR binding to actin filament deformations instead of myosin II directly (Fig. 4 *J* and *K*). In actomyosin contraction assays that lack the cross-linker α-actinin, myosin drives contraction of the F-actin network into asters, which are dense clusters of actin and myosin II. Previous work has shown that these so-called asters are sites where filaments are buckled and broken due to compressive forces (31). We observe that SNAP-LCR localizes to these asters, suggesting that LCR localization does not require the cross-linker α-actinin and localizes to highly compacted actomyosin (Fig. 4*L*). These data show that myosin II-generated forces on actin filaments is necessary and sufficient to drive LIM localization to actin filaments.

Polymerization-Generated Stress Is Sufficient for LCR Localization to Actin. To determine whether LCR localization can occur by alternate means of applying force to actin filaments, we employed a well-established reconstitution assay that serves as a model for actin-based motion (35, 36). Here, 2-μm polystyrene beads were coated with the Arp2/3 complex nucleation-promoting factor pWa (Fig. 5). Mixing the beads with actin monomers, Arp2/3 complex, and capping protein drives the assembly of a branched network of short actin filaments at the bead surface (37), which can be visualized by imaging of fluorescently labeled actin. In the expanding actin shell, the outer network continuously stretches as it is displaced outward by continuous assembly of new actin at the bead surface. Forces generated by actin polymerization result in the buildup of circumferential tension along the outer part of the actin shell, resulting in network tearing that breaks the symmetrical shell. After symmetry breaking, the so-called comet tail drives directed bead motion (35). Previous work has demonstrated that capping protein (CP) facilitates symmetry breaking, as short-capped filaments are more effective in force generation (38–40).

In the absence of capping protein, large amounts of actin are assembled from the bead that elongates away from the bead surface. While the overall actin signal is much higher in the absence of capping protein, LCR binds only slightly above background detection (Fig. 5 *A*–*C*). Conversely, in the presence of capping protein, we observed a wide distribution of LCR binding to the shell. A subset of beads has high LCR intensity associated with the actin shell (~50%), while others display levels of LCR binding similar to controls without capping protein (Fig. 5*C*). However, in this set of assays, the high concentration of capping protein inhibits formation of a complete actin shell on the bead, and we witness no instances of symmetry breaking. In confocal sections taken through the center of beads in the presence of a lower concentration of capping protein, the LCR localizes where the actin signal is weakest (Fig. 5 *D* and *E*). We speculate this is because symmetry begins to break at these sites and the F-actin network thins as it is strained. To look more closely at this phenomenon, we took confocal time-lapse movies of beads going through the process of symmetry breaking. We observed the LCR localizing most intensely to the actin shell during the period of most rapid straining as the shell ruptures (Fig. 5*D* and Movie S8).

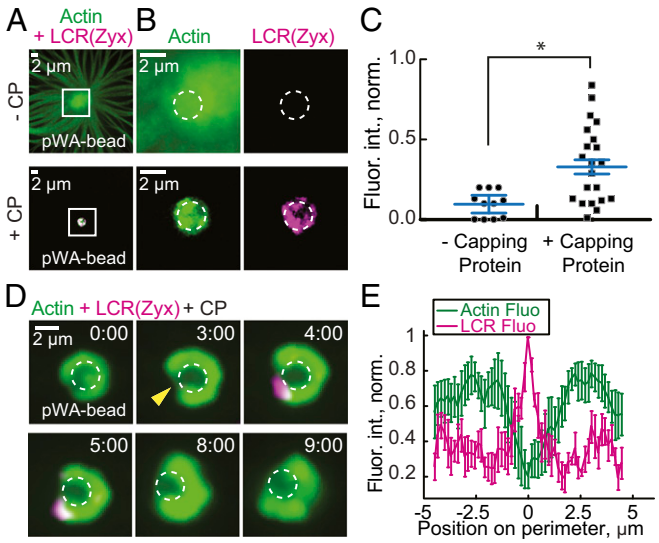

Fig. 5. SNAP-LCR(zyx) localizes to branched F-actin networks during symmetry breaking. (*A*–*C*) LCR(zyx) localizes to capped F-actin networks in motile bead assays. (*A*) Confocal images taken from a motile bead assay, where the Arp2/3 complex activator pWa is electrostatically bound to the surface of polystyrene beads. The beads are mixed with 4 μM actin monomer (5% Alexa-488 labeled), 100 nM Arp2/3 complex, 12 μM profilin, and 400 nM LCR(zyx) in polymerization buffer in the presence or absence of 200 nM capping protein. (*B*) Zoomed images from the white boxed region of *A*. White circle traces the beads. (*C*) LCR fluorescence on the actin networks in *A* in the absence or presence of capping protein. Normalization was done relative to the total actin fluorescence on the bead. $n > 10$, error bars = SEM; $^*P < 0.05$ as determined from *t* test. (*D* and *E*) HALO-LCR(zyx) localizes to symmetry breaking events in motile bead assays. The pWa beads are mixed with 2 μM actin monomer (5% Alexa-488 labeled), 100 nM Arp2/3 complex, 100 to 200 nM LCR(zyx), and 42 nM capping protein. (*D*) Confocal time lapse of a representative symmetry breaking event. White circle indicates the beads, and the yellow arrow shows where symmetry breaks. (*E*) Linescans of LCR (magenta) and actin (green) fluorescence on the circumference of the F-actin network from reactions where beads break symmetry. Linescans are the average of five beads and were aligned by setting the peak LCR intensity to position zero. Error bars = SEM.

Discussion

Here we show that the mechanism by which zyxin is recruited to SFSS is through binding of its LCR exclusively to mechanically strained actin filaments and note that a parallel study has come to the same conclusion independently (28). We identify 18 proteins from four different LIM domain protein classes with LCRs that localize to SFSS, indicating that this force-sensitive interaction may function as an input into diverse cellular processes. While SFSS are a particular feature within adherent fibroblasts, mechanical stresses are ubiquitous within the actin cytoskeleton. Force-sensitive biochemistry is inherent to mechanical regulation of the cytoskeleton and, we suspect, also a means for transmitting information about the mechanical status of the cell to the nucleus. The tension in SFs tends to reflect the mechanics of the environment in which cells are embedded. Cells growing in rigid matrices or within tissues that are being stretched build F-actin networks under increased tension (1, 19, 41). Recent work suggests that matrix mechanics and the resulting actin networks control nuclear localization of the LIM protein FHL2 (28, 42).

Interestingly, a majority of SFSS-binding LIM proteins display nuclear shuttling (43), suggesting a model by which LCR binding to stressed F-actin networks blocks nuclear import. Our data raise the possibility that detection of cytoskeletal mechanics by LCRs from four different LIM classes (22), Zyxin, Paxillin, Tes, and Enigma, may underlie regulation of diverse transcriptional pathways they are part of, including YAP/TAZ, Hippo, p21 signaling, and planer cell polarity. While much work has demonstrated these to be mechanically regulated (1, 42, 44, 45), our work implicates interactions between the LCR with strained actin filaments in diverse cytoskeletal assemblies as a potential mechanism. We anticipate that understanding the details of how and why diverse LIM domain-containing proteins differentially localize to strained actin filaments at focal adhesions, cell–cell adhesions, and the actin cytoskeleton will yield insight into the regulation and architecture of these mechanotransduction pathways (Fig. 6*A*).

In vitro data from both this and a parallel study (28) indicate that the LCR can be recruited to highly tensed or compressed actin filaments, suggesting that these two distinct force-induced filament conformations may expose a similar actin filament structure that has high affinity for the LCR (Fig. 6*B*). The maximum distortion that may occur within a highly bent filament before it breaks is estimated to be ∼1.5 Å of displacement/subunit (46). An attractive hypothesis is that mechanical stretch, compression, or twist exposes a site within the actin filament that is weakly recognized by each LIM domain. Future work is needed to understand the full mechanism of the force-dependent interaction. A parallel study identified a phenylalanine within each LIM domain that was necessary for force-dependent association with actin filaments (28). Both Sun et al. (28)'s and our data demonstrate this site is not sufficient, as tandem LIM domains are required. Our work suggests that three tandem domains connected by linkers of a precise length, each contribute to binding a strained-induced feature on an actin filament. We suspect the linker length may act as a ruler that positions individual LIM domains to optimally bind a stress-induced feature on the actin filament (Fig. 6*B*).

We show that this force sensitivity is found in fission yeast LIM protein Pxl1. The fact that Pxl1 both localizes to the contractile ring in fission yeast and to SFSS in animal cells suggests that myosin II-induced strained actin filament conformations are a common feature in contractile networks. Despite large evolutionary distances, this interaction has been conserved, indicating that there is significant selective pressure to maintain it. Actin is one of the most highly conserved proteins in eukaryotes with 90.4% amino acid sequence identity between fission yeast and mammals, so it is not surprising that the LCR of Pxl1 from fission yeast binds to a strained F-actin structure in mammals. The oldest LIM domain protein found in plants and animals, CRP (22), binds and bundles actin filaments via its LIM domains in the absence of mechanical stress (47–49). We hypothesize that duplication and divergence of an ancestral CRP-like LIM domain resulted in a modification to its actin-binding mechanism that favored a strained conformation of F-actin (Fig. 6*C*). The other core components of the contractile machinery, myosin II and α-actinin, have not been found in plants but are clearly present in the unikonts (50, 51) and may have appeared around similar times. We hypothesize that the emergence of contractile F-actin machinery coincided with, or required proteins that

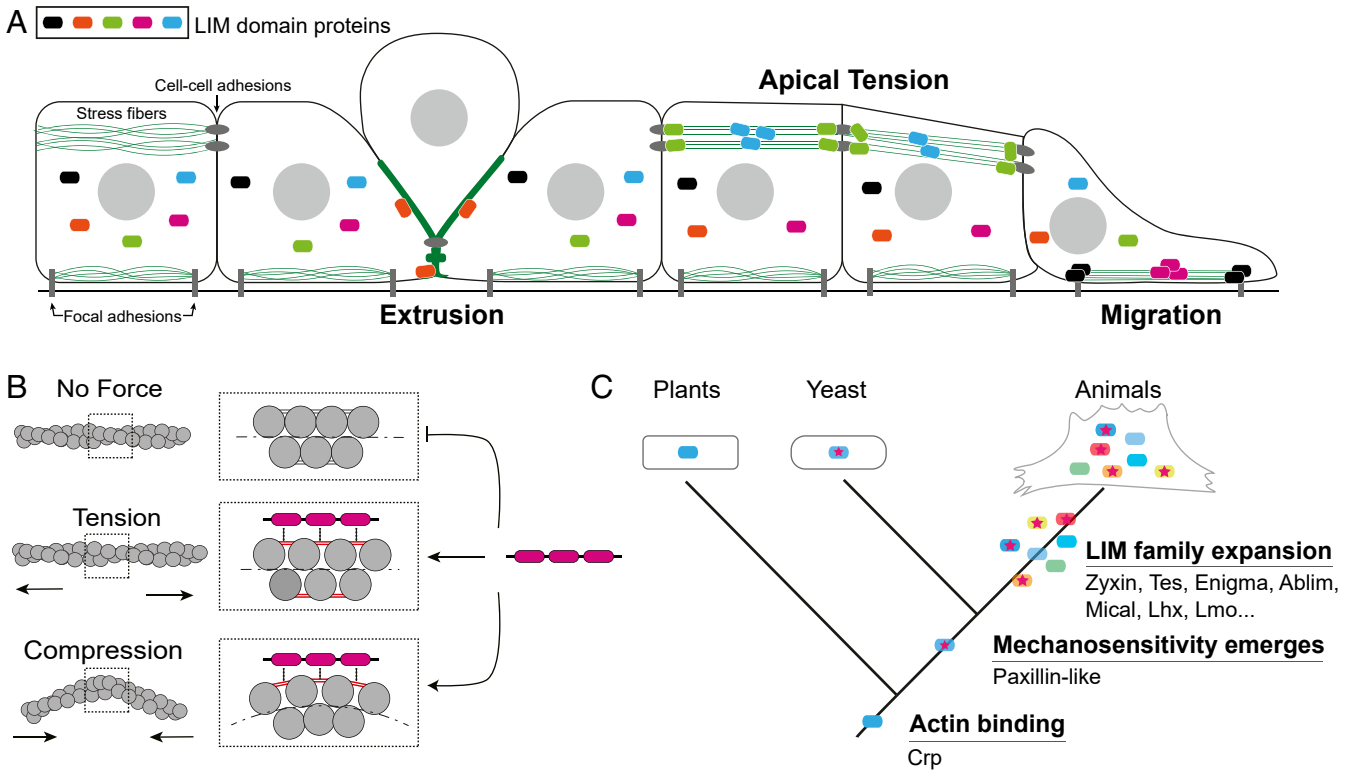

Fig. 6. Model. (*A*) Cartoon of an epithelial tissue layer with different examples of mechanical stress that cells experience (extrusion, apical tension, and migration). LIM domains bind the different mechanically stressed F-actin networks. (*B*) Actin filament experiencing different forces: tension (*Middle*) or bending due to compression which is likely coupled to changes in filament twist (*Bottom*). The box indicates the zoomed in diagram showing the bonds between actin subunits. The gray lines indicate regions of low stress while the red lines indicate high stress due to tension, compression, or twist-bend coupling. LIM domain proteins likely localize through their LCR to the regions of high stress. (*C*) Phylogenetic tree showing emergence of strained actin filament binding by paxillin class of LIM domain proteins and later expansion of LIM family in the metazoan stem lineage.

could report on the stresses present there. The oldest SFSS-binding class from our screen appears to be paxillin (22), which is involved in mechanical homeostasis of contractile networks in yeast (26) and mammals (18). F-actin strain sensing via LIM may have been co-opted by other signaling pathways later on during the LIM family expansion that originated in the stem lineage of metazoans (Fig. 6*C*) (22).

Zinc finger proteins have diverse functionality from regulation of cell cycle, transcription, and protein folding through interactions with DNA, lipids, and proteins (52). Our data demonstrate that mechanically stressed actin filaments are an additional substrate for a subset of zinc finger proteins. The extent to which mechanical forces may regulate interactions with other known substrates is an opportunity to be explored. The use of the actin filament itself as a force sensor, or mechanophore, within the actin cytoskeleton is a particularly attractive one as a means to control mechanotransduction pathways. Both its abundance and the different types of force (twist, compression, extension) that can be sensed could provide a wealth of control of mechanotransduction pathways. Moreover, our work suggests the possibility of other biomolecules that exclusively bind to mechanically stressed filaments that may not have been isolated by traditional biochemical studies.

Materials and Methods

SFSS were analyzed by measuring the ratio of the mean fluorescence of transiently transfected mCherry-tagged LCRs to the stably integrated EGFP-zyxin fluorescence imaged via confocal microscopy. Background was considered to be the location on the stress fiber where the SFSS eventually developed. Kymographs were generated with ImageJ reslice function, or if stress fibers moved significantly, a python script written in ImageJ from user-drawn line segments was used. For in vitro contractility assays, time-lapse TIRFM movies were obtained of bundled actin networks consisted of F-actin (1.5 or 3 μM, 10% Alexa-488 labeled), α-actinin (100 to 200 nM), LCR (50 to 200 nM), and polymerization TIRF buffer. To induce network contraction, polymerized myosin (50 to 150 nM) was flowed into the chamber. Details of all methods and protocols are found in *SI Appendix*.

Data Availability. Supporting data and plasmids from this study will be made available from the corresponding authors upon reasonable request and through Addgene (https://www.addgene.org). Code will be made available on GitHub (https://github.com).

ACKNOWLEDGMENTS. We thank Mary Beckerle and her laboratory for the GFP-zyxin fibroblasts. We thank Greg Alushin, Mary Beckerle, and Clare Waterman for helpful discussions and exchange of preliminary data over the last several years. We acknowledge funding from NIH R01 GM104032 (M.L.G.), NIH R01 GM079265 (D.R.K.), Army Research Office Multi University Research Initiative (ARO MURI) W911NF1410403 (M.L.G. and D.R.K.), NIH F32 GM122372 (J.D.W.), and NIH MCB Training Grant T32 GM0071832 (C.A.A.). This work was partially supported by the University of Chicago Materials Research Science and Engineering Center, funded by the National Science Foundation under award numbers DMR-1420709 and DMR-2011854.

1. C. Rauskolb, S. Sun, G. Sun, Y. Pan, K. D. Irvine, Cytoskeletal tension inhibits Hippo signaling through an Ajuba-Warts complex. *Cell* **158**, 143–156 (2014).
2. S. Huang, D. E. Ingber, The structural and mechanical complexity of cell-growth control. *Nat. Cell Biol.* **1**, E131–E138 (1999).
3. Y. S. Chatzizisis *et al*., Role of endothelial shear stress in the natural history of coronary atherosclerosis and vascular remodeling: Molecular, cellular, and vascular behavior. *J. Am. Coll. Cardiol.* **49**, 2379–2393 (2007).
4. N. Ohura *et al*., Global analysis of shear stress-responsive genes in vascular endothelial cells. *J. Atheroscler. Thromb.* **10**, 304–313 (2003).
5. D. R. Carter, G. S. Beaupré, N. J. Giori, J. A. Helms, Mechanobiology of skeletal regeneration. *Clin. Orthop. Relat. Res.* (suppl. 355), S41–S55 (1998).
6. Z. Sun, S. S. Guo, R. Fässler, Integrin-mediated mechanotransduction. *J. Cell Biol.* **215**, 445–456 (2016).
7. J.-C. Kuo, X. Han, C.-T. Hsiao, J. R. Yates 3rd, C. M. Waterman, Analysis of the myosin-II-responsive focal adhesion proteome reveals a role for β-Pix in negative regulation of focal adhesion maturation. *Nat. Cell Biol.* **13**, 383–393 (2011).
8. H. B. Schiller, C. C. Friedel, C. Boulegue, R. Fässler, Quantitative proteomics of the integrin adhesome show a myosin II-dependent recruitment of LIM domain proteins. *EMBO Rep.* **12**, 259–266 (2011).
9. L. M. Owen, N. A. Bax, W. I. Weis, A. R. Dunn, The C-terminal domain of talin forms a force-responsive, directional catch bond to F-actin. *Biophys. J.* **118**, 31a (2020).
10. D. L. Huang, N. A. Bax, C. D. Buckley, W. I. Weis, A. R. Dunn, Vinculin forms a directionally asymmetric catch bond with F-actin. *Science* **357**, 703–706 (2017).
11. T. D. Pollard, L. Blanchoin, R. D. Mullins, Molecular mechanisms controlling actin filament dynamics in nonmuscle cells. *Annu. Rev. Biophys. Biomol. Struct.* **29**, 545–576 (2000).
12. P. Bieling *et al*., Force feedback controls motor activity and mechanical properties of self-assembling branched actin networks. *Cell* **164**, 115–127 (2016).
13. V. I. Risca *et al*., Actin filament curvature biases branching direction. *Proc. Natl. Acad. Sci. U.S.A.* **109**, 2913–2918 (2012).
14. K. Hayakawa, H. Tatsumi, M. Sokabe, Actin filaments function as a tension sensor by tension-dependent binding of cofilin to the filament. *J. Cell Biol.* **195**, 721–727 (2011).
15. H. Wioland, A. Jegou, G. Romet-Lemonne, Torsional stress generated by ADF/cofilin on cross-linked actin filaments boosts their severing. *Proc. Natl. Acad. Sci. U.S.A.* **116**, 2595–2602 (2019).
16. V. E. Galkin, A. Orlova, E. H. Egelman, Actin filaments as tension sensors. *Curr. Biol.* **22**, R96–R101 (2012).
17. L. M. Hoffman, C. C. Jensen, A. Chaturvedi, M. Yoshigi, M. C. Beckerle, Stretch-induced actin remodeling requires targeting of zyxin to stress fibers and recruitment of actin regulators. *Mol. Biol. Cell* **23**, 1846–1859 (2012).
18. M. A. Smith *et al*., LIM domains target actin regulators paxillin and zyxin to sites of stress fiber strain. *PLoS One* **8**, e69378 (2013).
19. M. Yoshigi, L. M. Hoffman, C. C. Jensen, H. J. Yost, M. C. Beckerle, Mechanical force mobilizes zyxin from focal adhesions to actin filaments and regulates cytoskeletal reinforcement. *J. Cell Biol.* **171**, 209–215 (2005).
20. M. A. Smith *et al*., A zyxin-mediated mechanism for actin stress fiber maintenance and repair. *Dev. Cell* **19**, 365–376 (2010).
21. M. A. Smith, L. M. Hoffman, M. C. Beckerle, LIM proteins in actin cytoskeleton mechanoresponse. *Trends Cell Biol.* **24**, 575–583 (2014).
22. B. J. Koch, J. F. Ryan, A. D. Baxevanis, The diversification of the LIM superclass at the base of the metazoa increased subcellular complexity and promoted multicellular specialization. *PLoS One* **7**, e33261 (2012).
23. S. Tojkander, G. Gateva, P. Lappalainen, Actin stress fibers–assembly, dynamics and biological roles. *J. Cell Sci.* **125**, 1855–1864 (2012).
24. J.-Q. Wu *et al*., Assembly of the cytokinetic contractile ring from a broad band of nodes in fission yeast. *J. Cell Biol.* **174**, 391–402 (2006).
25. M. Pinar, P. M. Coll, S. A. Rincón, P. Pérez, Schizosaccharomyces pombe Pxl1 is a paxillin homologue that modulates Rho1 activity and participates in cytokinesis. *Mol. Biol. Cell* **19**, 1727–1738 (2008).
26. W. Ge, M. K. Balasubramanian, Pxl1p, a paxillin-related protein, stabilizes the actomyosin ring during cytokinesis in fission yeast. *Mol. Biol. Cell* **19**, 1680–1692 (2008).
27. T. H. Cheffings, N. J. Burroughs, M. K. Balasubramanian, Actin turnover ensures uniform tension distribution during cytokinetic actomyosin ring contraction. *Mol. Biol. Cell* **30**, 933–941 (2019).
28. X. Sun *et al*., Mechanosensing through direct binding of tensed F-actin by LIM domains. *Dev. Cell*, 10.1016/j.devcel.2020.09.022 (2020).
29. P. B. Harbury, T. Zhang, P. S. Kim, T. Alber, A switch between two-, three-, and four-stranded coiled coils in GCN4 leucine zipper mutants. *Science* **262**, 1401–1407 (1993).
30. T. D. Pollard, Actin and actin-binding proteins. *Cold Spring Harb. Perspect. Biol.* **8**, 018226 (2016).
31. M. P. Murrell, M. L. Gardel, F-actin buckling coordinates contractility and severing in a biomimetic actomyosin cortex. *Proc. Natl. Acad. Sci. U.S.A.* **109**, 20820–20825 (2012).
32. M. Murrell, T. Thoresen, M. Gardel, Reconstitution of contractile actomyosin arrays. *Methods Enzymol.* **540**, 265–282 (2014).
33. E. M. De La Cruz, J. Roland, B. R. McCullough, L. Blanchoin, J.-L. Martiel, Origin of twist-bend coupling in actin filaments. *Biophys. J.* **99**, 1852–1860 (2010).
34. T. D. Pollard, A guide to simple and informative binding assays. *Mol. Biol. Cell* **21**, 4061–4067 (2010).
35. T. P. Loisel, R. Boujemaa, D. Pantaloni, M. F. Carlier, Reconstitution of actin-based motility of Listeria and Shigella using pure proteins. *Nature* **401**, 613–616 (1999).
36. M. J. Dayel *et al*., In silico reconstitution of actin-based symmetry breaking and motility. *PLoS Biol.* **7**, e1000201 (2009).
37. V. Achard *et al*., A "primer"-based mechanism underlies branched actin filament network formation and motility. *Curr. Biol.* **20**, 423–428 (2010).
38. A. Bernheim-Groswasser, S. Wiesner, R. M. Golsteyn, M.-F. Carlier, C. Sykes, The dynamics of actin-based motility depend on surface parameters. *Nature* **417**, 308–311 (2002).

39. M. J. Dayel *et al*., In silico reconstitution of actin-based symmetry breaking and motility. *PLoS Biol.* **7**, e1000201 (2009).
40. A. Mogilner, On the edge: Modeling protrusion. *Curr. Opin. Cell Biol.* **18**, 32–39 (2006).
41. L. Kurzawa *et al*., Dissipation of contractile forces: The missing piece in cell mechanics. *Mol. Biol. Cell* **28**, 1825–1832 (2017).
42. N. Nakazawa, A. R. Sathe, G. V. Shivashankar, M. P. Sheetz, Matrix mechanics controls FHL2 movement to the nucleus to activate p21 expression. *Proc. Natl. Acad. Sci. U.S.A.* **113**, E6813–E6822 (2016).
43. J. L. Kadrmas, M. C. Beckerle, The LIM domain: From the cytoskeleton to the nucleus. *Nat. Rev. Mol. Cell Biol.* **5**, 920–931 (2004).
44. S. Dupont *et al*., Role of YAP/TAZ in mechanotransduction. *Nature* **474**, 179–183 (2011).
45. A. Vichas, J. A. Zallen, Translating cell polarity into tissue elongation. *Semin. Cell Dev. Biol.* **22**, 858–864 (2011).
46. Y. Arai *et al*., Tying a molecular knot with optical tweezers. *Nature* **399**, 446–448 (1999).
47. R. Weiskirchen, K. Günther, The CRP/MLP/TLP family of LIM domain proteins: Acting by connecting. *BioEssays* **25**, 152–162 (2003).
48. T. C. Tran, C. Singleton, T. S. Fraley, J. A. Greenwood, Cysteine-rich protein 1 (CRP1) regulates actin filament bundling. *BMC Cell Biol.* **6**, 45 (2005).
49. M. Grubinger, M. Gimona, CRP2 is an autonomous actin-binding protein. *FEBS Lett.* **557**, 88–92 (2004).
50. T. A. Richards, T. Cavalier-Smith, Myosin domain evolution and the primary divergence of eukaryotes. *Nature* **436**, 1113–1118 (2005).
51. M. Lek, D. G. MacArthur, N. Yang, K. N. North, Phylogenetic analysis of gene structure and alternative splicing in α-actinins. *Mol. Biol. Evol.* **27**, 773–780 (2010).
52. J. H. Laity, B. M. Lee, P. E. Wright, Zinc finger proteins: New insights into structural and functional diversity. *Curr. Opin. Struct. Biol.* **11**, 39–46 (2001).